A pruning algorithm for polycrystalline data in high performance computing

Harris Farooq, David Ryckelynck, Samuel Forest, Georges Cailletaud, Aldo Marano

Noname manuscript No.
(will be inserted by the editor)

A pruning algorithm for polycrystalline data in high performance computing

Harris Farooq · David Ryckelynck · Samuel Forest · Georges Cailletaud · Aldo Marano

Received: 01/21/2021 / Accepted: date

Abstract We are exploring the idea of data pruning via hyperreduction modeling. The proposed algorithm preserves data driven modeling capabilities while reducing storage resources. High resolution crystal plasticity finite element simulations demand huge computational and storage resources, especially in cases where hundreds of grains are interacting under cyclic loading. The development of image-based modeling via computed tomography highlights the problem of long-term storage of simulation data. The present paper focuses on modeling cyclic strain-ratcheting as an example of numerical modeling that the proposed algorithm preserves. The size of the remaining sampled data can be user-defined, depending on the needs concerning storage space. The pruning algorithm can be supplemented by data compression, but con-

H. farooq
MINES ParisTech, PSL University, MAT-Centre des matériaux, CNRS UMR 7633, BP 87 91003 Evry, France
E-mail: hf354@cam.ac.uk
Present address: of H. Farooq

D. Ryckelynck
MINES ParisTech, PSL University, MAT-Centre des matériaux, CNRS UMR 7633, BP 87 91003 Evry, France
E-mail: david.ryckelynck@mines-paristech.fr

S. Forest
MINES ParisTech, PSL University, MAT-Centre des matériaux, CNRS UMR 7633, BP 87 91003 Evry, France
E-mail: samuel.forest@mines-paristech.fr

G. Cailletaud
MINES ParisTech, PSL University, MAT-Centre des matériaux, CNRS UMR 7633, BP 87 91003 Evry, France
E-mail: georges.cailletaud@mines-paristech.fr

A. Marano
MINES ParisTech, PSL University, MAT-Centre des matériaux, CNRS UMR 7633, BP 87 91003 Evry, France
E-mail: aldo.marano@mines-paristech.fr

trary to usual compression algorithms large data reduction is obtained for the price of reasonable approximation errors. The proposed data pruning procedure is deeply linked to hyperreduction techniques. As a result, a pruned microstructure equipped with latent variables is generated. The data outside the pruned microstructure are either deleted or encoded with reduced bases. The approximate recovery of the original data follows the physical equations involved in a hyperreduced model. It fosters extrapolation of pruned data. In this paper the extrapolation is conducted over 190 cycles for input data covering 10 cycles only over a pruned microstructure. Because of the cyclic strain-ratcheting nature of the problem, approximation errors may be accumulated over cycles. The relevance of the pruned data is tested afterwards for statistics on the predicted strain field, as if full finite element data were available.

Keywords Model order reduction · CPFEM · Ratcheting · Data compression · Pruning algorithm · Material database

1 Introduction

With the development and the generalization of Computed Tomography (CT), the volume of data acquired has drastically increased. This raises new challenges, such as data storage, data mining or the development of relevant experiments-simulations dialog methods such as model validation and model calibration. When material microstructures are under consideration, continuum models can be an attractive approach to assess mechanical properties. Coupling micro-mechanical laws with complex geometries has in present times gained massive popularity [16,17]. This is followed by a numerical procedure to solve the boundary value problem. One of the most popular methods to discretize the weak form of constitutive equations is the Finite Element method, which is also employed in this article. Using this method, the constitutive equations can be integrated at each material point and huge insight can be gained as to what is happening locally at certain geometric locations for various parameter variations. In this context, of particular interest are strain-ratcheting simulations where plasticity accumulates at certain locations during cycling loading. Analyzing such a problem is crucial for lifetime assessment of engineering components. This requires considerable computational and storage resources for direct numerical simulations. The current state of computer science is considerably advanced, with numerous parallel as well as high performance computing strategies available [39,43]. But, full resolution simulations are now related to massive microstructural data. As a result, finite element simulations using X-ray CT data or synthetic microstructures [37] lead to an explosion of the volume of data to store.

Recently, databases of simulation data have demonstrated their viability and computational advantages for facilitating crystal plasticity predictions [1]. Obviously, much more can be expected from a database for crystal plasticity. It should foster: reproducibility as in other scientific domains [2], the training

of artificial neural networks [14] or Bayesian network [32], the exploration of new physical parameters or new assumptions, the detailed comparison between various materials, and additional model updating [19,38] when new observational data are available. Therefore, the long-term storage of a database in crystal plasticity is nowadays an issue.

Data compression/decompression schemes are already available in the framework of high performance computing [25]. Lossy compression allows the precision of the data to be reduced in a way that has an insignificant impact on the data. In [25], when applying their proposed compression scheme to data produced by the CHIME experiment, the data are compressed to 28% of their original size. The present paper aims to explore the idea of data pruning via numerical modeling in order to release more storage space when needed, as a complementary approach to data compression. It is based on feature extraction from data, which is an other way for lossy compression. It can be performed via clustering [23], linear dimensionality reduction or via autoencoders [14]. In [19], data pruning via linear dimensionality reduction and hyperreduction is shown to preserve simulation capabilities while reducing the storage resources. In the present paper, this data pruning strategy is evaluated for polycrystalline materials. Data outside a reduced domain are deleted. Full strain field are recovered via hyperreduced predictions supplemented by a Gappy POD procedure [9].

Hyperreduction methods belong to projection-based model order reduction methods (PBMORs) via linear dimensionality reduction. PBMOR methods pertain to problems where the simulation data that we wish to produce belongs to a small vector space (i.e. having a small dimension) and when the quantity of interest is not well establish prior doing any numerical prediction, and may require more data extrapolation or exploration. Several authors [26] have proposed model reduction techniques for the approximation of plasticity problems. For instance [30] proposed to use the LATIN method to iteratively approximate the solution, without using simulation data forecast by any finite element model. [15] use a space-time technique where a low number of nonlinear equations is solved in the reduced setting but full spatial information can be recovered at any given time. Access to recovered data enables to define quantities of interest as if finite element simulation had been performed. [28] have proposed to use the nonuniform transformation field analysis (NTFA) approach where they consider nonuniform plastic strain fields with the aim of reducing the number of macroscopic internal variables. Another model order reduction technique used frequently is proper orthogonal decomposition (POD), first proposed by [21] and [24] developed initially for statistical analyses. This POD basis comprises of the state subspace which are related to different time steps of a simulation or even different mechanical problems altogether. Using POD bases to predict mechanical models was first done by [29] for weather forecasts. In the above PBMOR methods, the reduced equations are setup on the full finite element mesh.

In PBMOR, a reduced basis is substituted for the usual finite element shape functions. Therefore dedicated numerical cubature schemes have been developed and named hyperreduction methods [33,10]. In hyperreduction PB-

MOR methods, the original mesh is sampled either at the level of integration points or at the level of elements. In [18], integration points are sampled for hyperreduced multiscale homogenization problems. In [33,34], the cubature is restricted to a reduced integration domain (RID). The RID is a subdomain of the original domain where the finite element equation are setup. This original domain can also be the one observed via CT. In [19], the reduced integration domain method have been used to prune tomographic data and related simulation data in the framework of model calibration for homogeneous materials undergoing strain localizations. The pruning procedure simply consists in deleting the data outside the RID, where the RID contains the finite elements connected to interpolation points computed by the discrete element interpolation (DEIM) [7] algorithm by considering the primal (displacement) reduced basis as well as the reduced basis generated using the strain field.

In this paper, it is shown that this pruning procedure preserves the capability of the ratcheting modeling in crystal plasticity. We restrict our attention to representative volume elements (RVE) where a virtual microstructural realization is generated and appropriate boundary conditions are prescribed [31,45, 22,41]. These boundary conditions usually represent an average stress or strain state of the material, which conforms to the macroscopic averaged response of the material.

The paper is organized in the following manner. In Section 2 the hyperreduction framework is explained. Section 3 presents the crystal plasticity material model, the finite element mesh description as well as the material model parameters used. Section 4 shows the setup of a cyclic simulation and Section 5 states the results and discussions. This is followed by the conclusions in Section 6.

2 Hyperreduction method for data pruning in computational mechanics of materials

In Finite Element (FE) models, the displacement field is decomposed over a set of vector functions $\boldsymbol{\varphi}_i(x)$ which correspond to the shape functions of the FE model defined on domain Ω.

$$\boldsymbol{u}(\boldsymbol{x},t) = \sum_{i=1}^{N_d} a_i(t)\boldsymbol{\varphi}_i(\boldsymbol{x}) \quad \forall\, \boldsymbol{x} \in \Omega \tag{1}$$

where N_d corresponds to the number of degrees of freedom of the mesh, t the time instant introduced for the solution of constitutive equations and a_i the i^{th} nodal degree of freedom of the FE model.

By following the Gappy POD method [9], any vector $\boldsymbol{a}$ belongings to column space of $\boldsymbol{V}$: *colspan*($\boldsymbol{V}$), can be recovered by using few entries of $\boldsymbol{a}$ denoted by $\boldsymbol{a}[\mathcal{F}]$, if $\boldsymbol{V}[\mathcal{F},:]$ is a full column rank matrix. *colspan*($\boldsymbol{V}$) is a linear latent space. It is usually obtained via the Snapshot POD [40] or a truncated singular value decomposition of a snapshot matrix containing training data.

Let's denote by $\boldsymbol{Q} \in \mathbb{R}^{N_d \times m}$ the snapshot matrix of finite element predictions: $Q_{ij} = a_i(t_j)$ where snapshots are selected at computational time instant $\{t_j\}_{j=1}^m$. It's truncated singular value decomposition reads:

$$\boldsymbol{Q} = \boldsymbol{V}\,\boldsymbol{S}\,\boldsymbol{W}^T + \boldsymbol{R}, \quad \boldsymbol{V}^T\,\boldsymbol{V} = \boldsymbol{W}^T\,\boldsymbol{W} = \boldsymbol{I}_N, \quad \boldsymbol{V}^T\boldsymbol{R} = 0 \tag{2}$$

where $\boldsymbol{S}$ is a diagonal matrix than contains the N_R largest singular values in decreasing order, $\boldsymbol{V} \in \mathbb{R}^{N_d \times N_R}$ and $\boldsymbol{W} \in \mathbb{R}^{m \times N_R}$ are orthogonal matrices, and $\boldsymbol{I}_{N_R}$ is the identity matrix of size N_R. $\boldsymbol{R} \in \mathbb{R}^{N_d \times m}$ is the residual of the decomposition.

The recovery procedure related to the Gappy POD reads:

$$\boldsymbol{a}^G = \boldsymbol{V}\,(\boldsymbol{V}[\mathcal{F},:]^T\,\boldsymbol{V}[\mathcal{F},:])^{-1}\,\boldsymbol{V}[\mathcal{F},:]^T\,\boldsymbol{a}[\mathcal{F}] \tag{3}$$

where $\boldsymbol{a}[\mathcal{F}]$ are pruned data, i.e. data restricted to a given subset of indices $\mathcal{F}$. When $\mathcal{F} = \mathcal{P}$, where $\mathcal{P}$ is the set of interpolation points for the columns of $\boldsymbol{V}$ by following the discrete empirical interpolation method (DEIM) [7,3], then $\boldsymbol{V}[\mathcal{P},:]$ is a square invertible matrix and the recovery procedure can be simplified as:

$$\boldsymbol{a}^{DEIM} = \boldsymbol{V}\,\boldsymbol{V}[\mathcal{P},:]^{-1}\,\boldsymbol{a}[\mathcal{P}] \tag{4}$$

When $\mathcal{F}$ contains interpolation points, $\mathcal{P} \subset \mathcal{F}$, the sub matrix $\boldsymbol{V}[\mathcal{F},:]$ is full column rank [12].

Property The Gappy POD recovery is the following oblique projection:

$$\boldsymbol{a} \in \mathbb{R}^{N_d}, \quad \boldsymbol{a}^G = \boldsymbol{V}\,(\boldsymbol{Z}^T\,\boldsymbol{V})^{-1}\,\boldsymbol{Z}^T\,\boldsymbol{a}, \qquad \boldsymbol{Z}^T = \boldsymbol{V}[\mathcal{F},:]^T\,\boldsymbol{I}_{N_d}[\mathcal{F},:] \tag{5}$$

Therefore, if $\boldsymbol{a} \in \mathit{colspan}(\boldsymbol{V})$ the recovered vector $\boldsymbol{a}^G$ is exact: $\boldsymbol{a}^G = \boldsymbol{a}$. Therefore the Gappy POD enables data pruning. The related pruned data are the reduced basis $\boldsymbol{V}$, the subset of indices $\mathcal{F}$ and the data restricted to this subset $\boldsymbol{a}[\mathcal{F}]$. But this pruning algorithm does not enable data extrapolation.

The hyperreduction method proposed in the framework of crystal plasticity in [36], is a convenient preprocessing step prior using the Gappy POD. It aims at predicting $\boldsymbol{a}[\mathcal{F}]$ by using physical governing equations and a projection on a vector subspace related to displacement field. This approach allows data extrapolation when predicting $\boldsymbol{a}[\mathcal{F}]$. Therefore, the pruned data via hyperreduction are $\boldsymbol{V}$, the subset of indices $\mathcal{F}$, and the data required to forecast $\boldsymbol{a}[\mathcal{F}]$. In the propose pruning algorithm, the recovery procedure start with the hyperreduced prediction of $\boldsymbol{a}[\mathcal{F}]$ and it is followed by the Gappy POD.

In essence, to set up the hyperreduced equations for a given FE model, this approach accounts for a low rank of the reduced approximation. For the sake of simplicity this can be elaborated using a linear elastic finite element model, or the linear step of a Newton Raphson algorithm, where the FE balance equation reads:

$$\boldsymbol{K}\boldsymbol{a}^{FE}(t) = \boldsymbol{c}(t) \tag{6}$$

where $\boldsymbol{a}^{FE} \in \mathbb{R}^{N_d}$, and $\boldsymbol{K} \in \mathbb{R}^{N_d \times N_d}$ is the tangent stiffness matrix of the FE model, whereas $\boldsymbol{c} \in \mathbb{R}^{N_d}$ the right hand side term of the FE equation. For

a given reduced basis of rank N_R, $\boldsymbol{V} \in \mathbb{R}^{N_d \times N_R}$, the approximate reduced solution of the balance equations is denoted by $\boldsymbol{a}^R$ as follows:

$$\boldsymbol{a}^R = \boldsymbol{V}\boldsymbol{b}^R \tag{7}$$

where $\boldsymbol{b}^R \in \mathbb{R}^{N_R}$ are reduced order model variables. In order to find a unique solution $\boldsymbol{b}^R$ the rank of $\boldsymbol{KV}$ needs to only be N_R. Since N_d is usually larger than N_R, a few rows of $\boldsymbol{KV}$ can be selected to preserve the rank of the sub-matrix. As proposed in [35], the hyperreduced balance equations are restricted to the RID using convenient test functions such that:

$$(\boldsymbol{V}[\mathcal{F},:])^T \boldsymbol{K}[\mathcal{F},:]\boldsymbol{V}\boldsymbol{b}^R = (\boldsymbol{V}[\mathcal{F},:])^T \boldsymbol{c}[\mathcal{F}] \tag{8}$$

The hyperreduced solution is denoted by $\boldsymbol{a}^{HR}$, $\boldsymbol{a}^{HR} = \boldsymbol{V}\boldsymbol{b}^R$. The RID is denoted by $\Omega_R \subset \Omega$. It is the support of the finite element shape functions $\boldsymbol{\varphi}_i$, for $i \in \mathcal{F}$:

$$\Omega_R = \cup_{i \in \mathcal{F}} \text{sup}(\boldsymbol{\varphi}_i) \tag{9}$$

Also, the RID must be large enough to have $\text{rank}(\boldsymbol{K}[\mathcal{F},:]\boldsymbol{V}) = N_R$; hence cardinality of the number of degrees of freedom in the RID should be greater than or equal to N_R.

The RID construction follows the heuristic rule: the extent of the RID must enable the recovery of the finite element displacement fields and the finite element strains when they both belongs to *colspan*($\boldsymbol{V}$) and *colspan*($\boldsymbol{V}^\epsilon$) respectively, where $\boldsymbol{V}^\epsilon$ is a reduced order basis for strain approximation. The set of interpolation points related to $\boldsymbol{V}^\epsilon$ is denoted by $\mathcal{P}^\epsilon$. The number of interpolation points is equal to the number of empirical modes in the reduced basis. By following the k-SWIM algorithm proposed in [19], the set $\mathcal{P}$ and $\mathcal{P}^\epsilon$, are not restrained to interpolation points of reduced bases. The number of points in this set is extended by a factor k. The k-SWIM points are more spread on Ω than the DEIM points. This algorithm is in the appendix 1. When $k = 1$ the k-SWIM points are the DEIM points. In addition, for each set of points $\mathcal{P}$ and $\mathcal{P}^\epsilon$ build by k-SWIM, we extract from the finite element mesh the degrees of freedom of the elements that contains the points in $\mathcal{P}$ and the points in $\mathcal{P}^\epsilon$. These sets of degrees of freedom are denoted $\mathcal{P}^+$ and $\mathcal{P}^{\epsilon+}$ respectively. In many practical situations, $\mathcal{F}$ also includes the degrees of freedom of a zone of interest. These degrees of freedom are denoted by $\mathcal{F}_o$. Therefore, we obtain the following set of degrees of freedom:

$$\mathcal{F} = \mathcal{F}_o \cup \mathcal{P}^+ \cup \mathcal{P}^{\epsilon+} \tag{10}$$

$\Omega \backslash \Omega_R$ is is counterpart of Ω_R. We denote by Γ^I the interface between Ω_R and $\Omega \backslash \Omega_R$. Let's introduce, $\mathcal{I}$, the set of degrees of freedom indices related to the interface Γ^I:

$$\mathcal{I} = \left\{ i \in \{1, ..., N_d\} \mid \int_{\Gamma^I} \boldsymbol{\varphi}_i^T \,.\, \boldsymbol{\varphi}_i \; d\Gamma \neq 0 \right\} \tag{11}$$

The matrix $\boldsymbol{K}$ is sparse. In the sequel, we assume that non zero entries in $\boldsymbol{K}[\mathcal{F},:]$ are only in the submatrix $\boldsymbol{K}[\mathcal{F},\mathcal{F}\cup\mathcal{I}]$ and these entries can be computed by using solely the reduced mesh that covers Ω_R. This assumption is too strong in case of contact problems as shown in [12]. So we restrict our attention to contact less problems for the sake of simplicity. More details on the hyperreduction of contact problems are available in [12].

Property If the hyperreduced matrix $(\boldsymbol{V}[\mathcal{F},:])^T\boldsymbol{K}[\mathcal{F},:]\boldsymbol{V}$ is full rank, the hyperreduced prediction $\boldsymbol{a}^{HR}$ is the following oblique projection of $\boldsymbol{a}^{FE}$:

$$\boldsymbol{a}^{HR} = \boldsymbol{V}\,(\boldsymbol{A}^T\boldsymbol{V})^{-1}\,\boldsymbol{A}^T\,\boldsymbol{a}^{FE} \tag{12}$$

where $\boldsymbol{A}^T = (\boldsymbol{V}[\mathcal{F},:])^T\boldsymbol{K}[\mathcal{F},:]$.

Obviously, this projection is performed via hyperreduced balance equations, without knowing $\boldsymbol{a}^{FE}$. It is a model that allows data extrapolation. The proof is straightforward because $\boldsymbol{A}^T\boldsymbol{V}$ is the hyperreduced matrix and $\boldsymbol{A}^T\,\boldsymbol{a}^{FE} = (\boldsymbol{V}[\mathcal{F},:])^T\boldsymbol{c}[\mathcal{F}]$. This projection is consistent because, if $\boldsymbol{a}^{FE} \in$ *colspan*$(\boldsymbol{V})$, it exists $\boldsymbol{b}^{FE}$ such that $\boldsymbol{a}^{FE} = \boldsymbol{V}\boldsymbol{b}^{FE}$ therefore $\boldsymbol{b}^R = \boldsymbol{b}^{FE}$ and $\boldsymbol{a}^{HR} = \boldsymbol{a}^{FE}$.

Once the hyperreduced prediction is known, we have access to local strain tensors for points in Ω_R:

$$\boldsymbol{\varepsilon}(\boldsymbol{x},t) = \frac{1}{2}(\nabla^T\boldsymbol{u}^{HR} + \nabla\boldsymbol{u}^{HR}), \quad \boldsymbol{u}^{HR}(\boldsymbol{x},t) = \sum_{i=\mathcal{F}\cup\mathcal{I}} a_i^{HR}(t)\boldsymbol{\varphi}_i(\boldsymbol{x}), \quad \forall\,\boldsymbol{x}\in\Omega_R \tag{13}$$

These strain tensor are usually evaluated at Gauss point of the reduced mesh that covers Ω_R. Let's denote by $\boldsymbol{\alpha}$ the vector of all Gauss point values of strain tensor for the original finite element mesh. The hyperreduction predicts only few rows of this vector: $\boldsymbol{\alpha}[\mathcal{F}^\epsilon]$ where $\mathcal{F}^\epsilon$ contains the indices of strain components at Gauss points of the reduced mesh. The reduced bases $\boldsymbol{V}^\epsilon$ is obtained by the truncated singular value decomposition of a snapshot matrix that contains a collection of full vectors $\boldsymbol{\alpha}$ for the same selected computational time instants $\{t_j\}_{j=1}^m$ introduced for displacements. This snapshot matrix is denoted by $\boldsymbol{Q}^\epsilon$. It reads: $Q^\epsilon_{ij} = \alpha_i(t_j)$. The Gappy POD recovery of the full strain field, at Gauss points of the original finite element mesh, reads:

$$\boldsymbol{\alpha}^G = \boldsymbol{V}^\epsilon\,(\boldsymbol{V}^\epsilon[\mathcal{F}^\epsilon,:]^T\,\boldsymbol{V}^\epsilon[\mathcal{F}^\epsilon,:])^{-1}\,\boldsymbol{V}^\epsilon[\mathcal{F}^\epsilon,:]^T\,\boldsymbol{\alpha}[\mathcal{F}^\epsilon] \tag{14}$$

Such kind of rule can be obtained for all variable equipped with a reduced basis.

The reduced variables $\boldsymbol{b}^R$ can be seen as latent variables in which unnecessary complexity has been removed. Therefore, the data pruning via hyperreduction is the deletion of simulation data and all input data outside the RID, i.e. related to $\Omega\backslash\Omega_R$. The solution of the hyperreduced balance equation requires to save $\boldsymbol{V}[\mathcal{F}\cup\mathcal{I}]$ which is the restriction of the reduced basis to the RID. The recovery of the full strain field over Ω by using the Gappy POD requires to save the full strain modes $\boldsymbol{V}^\epsilon$ and $\mathcal{F}^\epsilon$. Once the full strain field is recovered, the solution of the constitutive equations gives access to all mechanical variables. In practice, the memory size required to save the strain modes

$\boldsymbol{V}^{\epsilon}$ is one order of magnitude larger than the mechanical data required for the setting of the hyperreduced equations. The smaller the number of strain modes the higher the data pruning, but the larger the approximation error of the recovering procedure.

3 Crystal plasticity model and finite element mesh description

Data pruning is very relevant for complex physics-based computational models. In the present work a small strain crystal plasticity formulation is used for the computation as most local strains remain below 5%. Each grain is considered as a single crystal and the displacement fields are supposed to be continuous at the grain boundaries whereas stress can be discontinuous. To ease the interpretation of the numerical results, a rate independent single crystal plasticity model recently proposed by [13] is used. Also, the model exclusively uses kinematic hardening because it governs ratcheting effect. In Nickel-baed superalloys for instance, kinematic hardening dominates isotropic hardening under cyclic loading conditions [8]. Face centered cubic (FCC) single crystal metallic materials comprising of N plastic slip systems, each having a slip system direction $\boldsymbol{l}^s$ and the normal to the slip plane $\boldsymbol{n}^s$ are considered. The partition of the strain tensor introduces an elastic and a plastic part, denoted by $\boldsymbol{\varepsilon}^e$ and $\boldsymbol{\varepsilon}^p$ respectively:

$$\boldsymbol{\varepsilon} = \boldsymbol{\varepsilon}^e + \boldsymbol{\varepsilon}^p \tag{15}$$

The Hooke law relates the stress tensor to the elastic strain tensor. For cubic elasticity, a fourth rank tensor of elastic moduli $\boldsymbol{C}$, involving three independent parameters, governs the elastic behavior.

$$\boldsymbol{\sigma} = \boldsymbol{C}\boldsymbol{\varepsilon}^e \tag{16}$$

The plastic strain rate results from the slip processes with respect to all active slip systems,

$$\dot{\boldsymbol{\varepsilon}}^p = \sum_{s=1}^{N} \dot{\gamma}^s \boldsymbol{m}^s \tag{17}$$

with $\boldsymbol{m}^s$ being the orientation term

$$\boldsymbol{m}^s = \frac{\boldsymbol{l} \otimes \boldsymbol{n}^s + \boldsymbol{n} \otimes \boldsymbol{l}^s}{2} \tag{18}$$

The amount of slip rate on each slip system is denoted by the variable $\dot{\gamma}^s$. The driving force for plastic slip on slip system s is the resolved shear stress, computed using Cauchy stress ($\boldsymbol{\sigma}$) according to:

$$\tau^s = \boldsymbol{\sigma} : \boldsymbol{m}^s = \sigma_{ij} m_{ij}^s \tag{19}$$

The yield criterion is a generalization of Schmid's law involving scalar hardening variables r^s and x^s according to [27].

$$f^s(\boldsymbol{\sigma}, x^s, r^s) = |\tau^s - x^s| - r^s \tag{20}$$

Here, r^s denotes the radius of the elastic domain in terms of the resolved shear stress and x^s is a scalar back-stress characterizing the center of the elastic range in the one-dimensional space of resolved shear stresses. In slip based crystal plasticity, there are N such elastic ranges. Plastic slip can occur only if the function f^s becomes positive. In [13], the rate of slip on each slip system follows a rate-independent formulation of the form:

$$\dot{\gamma}^s = \dot{\varepsilon} \left\langle \frac{f^s}{P} \right\rangle \operatorname{sign}(\tau^s - x^s) \tag{21}$$

where P is a positive constant having the units of stress and $\dot{\boldsymbol{\varepsilon}}$ is a non-negative homogeneous function of order one in the total strain rate. The Macauley brackets $\langle \bullet \rangle = \operatorname{Max}(0, \bullet)$ are used to distinguish the elastic range from the plastic one, depending on the sign of the yield function f^s. In this model, $\dot{\boldsymbol{\varepsilon}}$ is taken to be the total equivalent distortional strain rate:

$$\dot{\varepsilon} = \sqrt{\frac{2}{3}\dot{\boldsymbol{\varepsilon}}' : \dot{\boldsymbol{\varepsilon}}'}, \qquad \dot{\boldsymbol{\varepsilon}}' = \dot{\boldsymbol{\varepsilon}} - \frac{1}{3}(\operatorname{tr}(\dot{\boldsymbol{\varepsilon}}))\boldsymbol{I} \tag{22}$$

where $\dot{\boldsymbol{\varepsilon}}'$ is the deviatoric part of the total strain rate tensor $\dot{\boldsymbol{\varepsilon}}$ and : is the inner product for second order tensors. Since the rate of inelasticity is linear in the total equivalent strain rate $\dot{\boldsymbol{\varepsilon}}$, all the evolution equations in the proposed theory are homogeneous of order one in time, characterizing a rate-independent response. Also the rate of inelasticity is used for all states entailing no need for special treatment of loading and unloading conditions. Also the functional form of f and the evolution equations for isotropic (r^s) as well as kinematic (x^s) hardening remain unchanged. The cumulative slip variable v^s is defined for each slip system by the following evolution equation:

$$\dot{\mathrm{v}}^s = |\dot{\gamma}^s| \tag{23}$$

Evolution equations for the kinematic hardening variables are taken from [27] and [6]. The nonlinear kinematic hardening evolution law

$$\dot{x}^s = C\dot{\gamma}^s - D\dot{\mathrm{v}}^s x^s \tag{24}$$

depends on two material parameters, C and D. In the present paper, there is no isotropic hardening so that the variable r^s has a constant value r_0, which is the value of the initial resolved shear stress.

The finite element balance equation reads:

$$\int_\Omega \boldsymbol{\varepsilon}(\boldsymbol{\varphi}_i) : \boldsymbol{\sigma}\, dV - \int_{\partial_F \Omega} \boldsymbol{\varphi}_i \, \boldsymbol{F}\, d\Gamma = 0 \quad \forall\, i \in \{1, \ldots, N_d\} \tag{25}$$

where $\boldsymbol{F}$ are the Neumann boundary conditions imposed at the boundary $\partial_F \Omega$ and where $\boldsymbol{\sigma}$ is estimated via the finite element approximation of the strain tensor:

$$\boldsymbol{\varepsilon} \approx \sum_{i=1}^{N_d} \boldsymbol{\varepsilon}(\boldsymbol{\varphi}_i)\, a_i \tag{26}$$

Literature findings show that the macroscopic representation of a micro-heterogeneous metallic material can be achieved with as few as one hundred grains [20], but matching macroscopic properties is not the goal here. Rather, the aim here is to have a large enough statistical pool of information so that local material response can be analyzed. Of course computational limitations have to be acknowledged and extremely large polycrystals cannot be used. The crystal plasticity parameter set employed in this paper is given in table 1. This is the same parameter set as the one used in the statistical analysis performed in [11] for Nicke-based superalloy IN718.

Cubic elasticity	C_{1111} = 259600 MPa C_{1122} = 179000 MPa C_{1212} = 109600 MPa
Critical resolved shear stress	R_0 = 320 MPa
Kinematic hardening	C = 100000 MPa D = 1000
Overstress	P = 9 MPa

Table 1: The crystal plasticity parameter set being used

An implicit finite element code [44] is used to solve the problem where the global equilibrium is solved using a Newton-Raphson algorithm. Integration of constitutive equations at the Gauss points is performed using the second order Runge-Kutta method with automatic time stepping [5].

$\boldsymbol{\Sigma}$ is the spatial average of tensor $\boldsymbol{\sigma}$:

$$\boldsymbol{\Sigma} = \frac{1}{V} \int_{\Omega} \boldsymbol{\sigma}\, d\Omega \tag{27}$$

Ω is a cubic representative volume elements. The six faces of the RVE are denoted $Face_i^+$, $Face_i^-$, for i=1, 2, 3. $Face_i^+$ and $Face_i^-$ are opposite faces. Load controlled mixed boundary conditions were imposed on the geometry such that the traction vector: $\underset{\sim}{\boldsymbol{\sigma}}.\underline{\boldsymbol{n}}$ is prescribed such that:

$$\Sigma_{11} = \text{constant on } Face_1^+$$
$$u_1 = 0 \;\; \forall \underline{\boldsymbol{x}} \in Face_1^-$$

Trivial boundary conditions (free boundary conditions) are imposed on all opposing faces i.e.

$$\sigma_{21}n_1 = \sigma_{31}n_1 = 0 \;\; \forall \underline{\boldsymbol{x}} \in Face_1^+ \cup Face_1^-$$
$$\sigma_{12}n_2 = \sigma_{22}n_2 = \sigma_{32}n_2 = 0 \;\; \forall \underline{\boldsymbol{x}} \in Face_2^+ \cup Face_2^-$$
$$\sigma_{13}n_3 = \sigma_{23}n_3 = \sigma_{33}n_3 = 0 \;\; \forall \underline{\boldsymbol{x}} \in Face_3^+ \cup Face_3^-$$

These boudary conditions are complemented by suitable additional Dirichlet condition to fix the overall rigid body motion.

4 Example of data extrapolation from pruned data in cyclic crystal plasticity

4.1 Feature selection for data pruning

A thousand grain polycrystal was chosen as an example where figure 1 shows a meshed finite element geometry with mixed traction boundary conditions. This finite element mesh was generated using the Voronoi tessellation technique with the help of the software VORO++ [37]. The mesh consists of 1174719 nodes and 859848 reduced C8D10 quadratic tetrahedral elements. Each element consists of four Gauss points. The crystallographic orientations chosen were randomly distributed throughout the polycrystal. The stress loading Σ_{11} follows a triangular signal where $\max_t \Sigma_{11} = 1000$ MPa and $R_\Sigma = \frac{\min_t \Sigma_{11}(t)}{\max_t \Sigma_{11}(t)} = -0.85$. These boundary values have been chosen carefully in order to simulate strain-ratcheting, which is a strain accumulation during loading cycles.

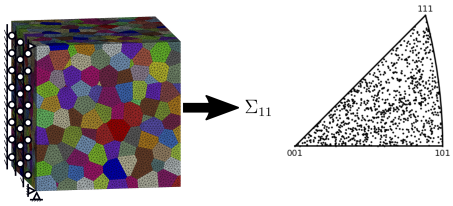

Fig. 1: A 1000 grains meshed microstructure with the inverse pole figure. Colors are related to grain orientations.

In order to show the extrapolation capabilities of the pruning algorithm via hyperreduction, the reduced bases are trained with simulation data related to the first ten loading cycles only. In the sequel, we show the ability of these reduced bases to predict up to 200 cycles. Figure 2 shows the local Euclidian norm for each displacement mode $\sum_{i=1}^{N_d} \boldsymbol{\varphi}_i(\boldsymbol{x})\, V_{ik}$ for $k = 1, \dots 6$. Figure 3 shows for each strain mode, the local von Mises strain $\epsilon_{vM} = \sqrt{\frac{3}{2}\boldsymbol{\epsilon}'_{ij}\boldsymbol{\epsilon}'_{ij}}$, where

$\boldsymbol{\epsilon}'$ is the deviatoric part of the local strain tensor. As anticipated, the magnitude of singular values exponentially decreases with the number of modes. For displacement 9 and for strain 20 modes are considered do get projection error of simulation data on reduced bases around 2%. This cutoff is arbitrary and dependent on the user. By looking at the contour plot of the modes in both cases it can be seen that the first few modes are homogeneously distributed while the later ones are high gradient modes. Also the modes of displacement decrease in magnitude more rapidly as compared to the modes of strain.

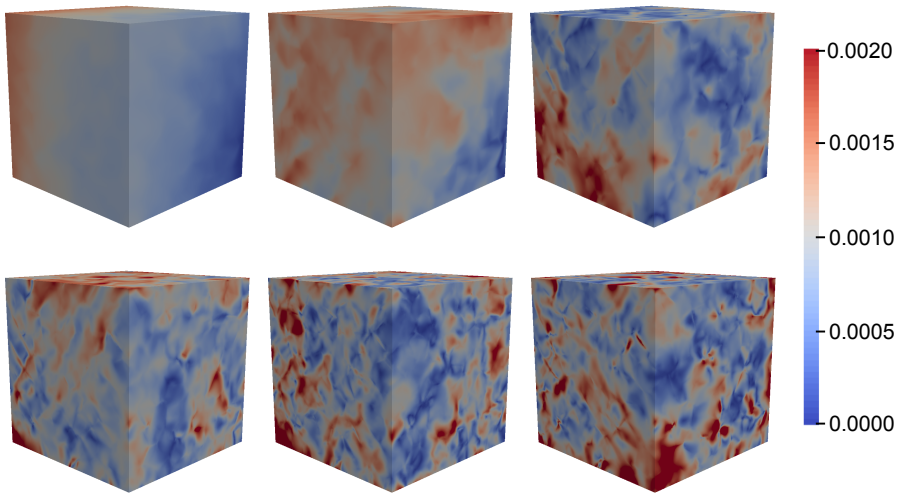

Fig. 2: Six first POD modes for displacement among 9 selected ($N = 9$) for the reduced basis $\boldsymbol{V}$. Here, the norm of local displacement vectors have been plot for each mode.

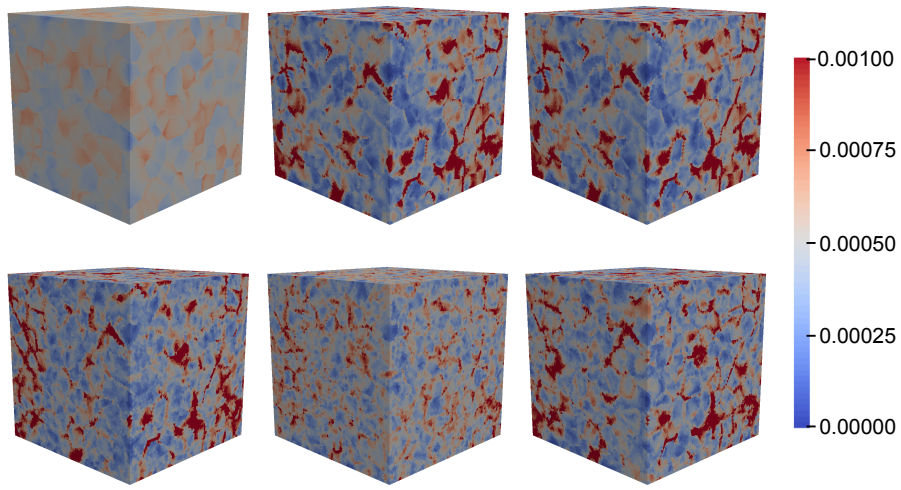

Fig. 3: Six first POD modes for strain field among 20 selected for the reduced basis $\boldsymbol{V}^{\epsilon}$. Here we have plot the local von Mises strain of each modes.

Figure 4 shows the reduced meshes constructed using the selected POD modes. A small RID have been obtained by the k-SWIM algorithm with $k = 1$ in Algorithm 1. With this setting $\mathcal{P}$ and $\mathcal{P}^{\epsilon}$ are the interpolation point of the DEIM algorithm. A large RID, with $k = 3$ in Algorithm 1, have been also generated. It contains more spread elements in Ω. The part of the finite element mesh provided in the zone of interest depends on which part of the mesh is the most critical according to the user. In the case being presented, a small central part of the boundary where pressure is being applied is included in the zone of interest, because this region experiences the most strain under a tensile load. Then it is a zone of interest.

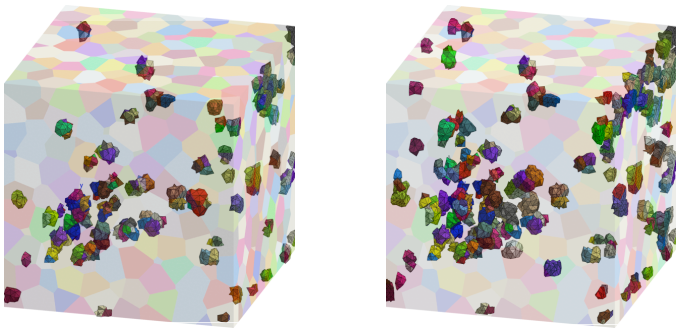

Fig. 4: On the left a small reduced integration domain restricted to 9300 finite elements, on the right a larger one involving 17400 finite elements. The original FE mesh is shown in transparency behind the RIDs. It contains 859848 elements. Colors are related to grain orientations.

The data to save in a storage system are summarized in Table 2, for three approach: the original data set, the Gappy POD, the hyperreduction. The data pruning using hyperreduction consists in saving a physical model. No FE simulation data is stored, only reduced bases. These reduced bases can obviously be supplemented by saving the reduced coordinates $\boldsymbol{b}^R$ related to displacement and also the one related to the strain field. These coordinates occupy a negligible memory size.

-	Data to save for $\overline{m}$ time steps
FE	$\{\boldsymbol{\alpha}^{FE}(t_j)\}_{j=1}^{\overline{m}}$
Gappy POD	$\{\boldsymbol{\alpha}^{FE}(t_j)[\mathcal{F}^\epsilon]\}_{j=1}^{\overline{m}}$, $\boldsymbol{V}^\epsilon$
Hyperreduction	Table 1, grain orientations in Ω_R, $\boldsymbol{V}^\epsilon$, $\boldsymbol{V}[\mathcal{F} \cup \mathcal{I}, :]$

Table 2: Data Pruning summary

4.2 Data extrapolation over 200 cycles

After constructing the reduced basis and the RIDs using an offline learning phase of just 10 cycles, recovery computations were performed via hyperreduction for two hundred stress controlled cycles. Let $\overline{m}$ denote the number of time steps involved in the recovery of the strain field for two hundred loading cycles. Here, $\overline{m} = 20\,m$, which represents an extrapolation of the original FE data over 190 loading cycles.

To compare the results, the original full field simulation was also run for two hundred cycles. Figure 5 shows recovered macroscopic data. It shows the

usual plot of macroscopic stress (Σ_{11}) vs the average strain (E_{11}) response of the three cases, hyperreduction using a small RID, hyperreduction using a large RID and the original data for comparison. To avoid clutter, responses are plotted only at cycles 1 and 200. It can be seen that the large RID is much better than the small RID at cycle 200. The pruning is more or less exact for the first 10 cycles for both RIDs, with error below 1% for all simulation data.

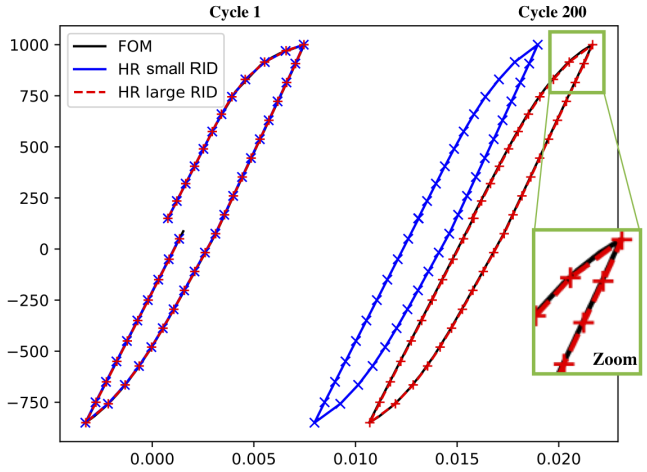

Fig. 5: Recovered macroscopic data. Macroscopic stress vs macroscopic strain response for cycle 1 and cycle 200 for the original FE prediction as well as the HROM for both the small RID and the large RID.

Statistics have been performed on local results that pertain to the time step taken at the tensile peak of cycle 200, after the recovery step of the full strain field by using: the Gappy POD applied to FE strains, the small RID, the large RID and the original FE data. The Gappy POD applied to FE strains requires to save the strain field in Ω_R over the 200 cycles as pruned data. It is more memory demanding. Figure 6 shows the kernel of the probability density function for ε_{11}, estimated from Gauss point values by using the method proposed in [4]. This method is available in Scipy [42]. The strain distribution plots show that locally the recovery of the full strain field via hyperreduction over a large RID is much better than using a small RID or the Gappy POD. The oblique projection involved in hyperreduction appears to be more accurate than the oblique projection performed by the Gappy POD. The former include physical equations the latter does not. Average values of local strain ε_{11} and the standard deviation are reported in Table 3.

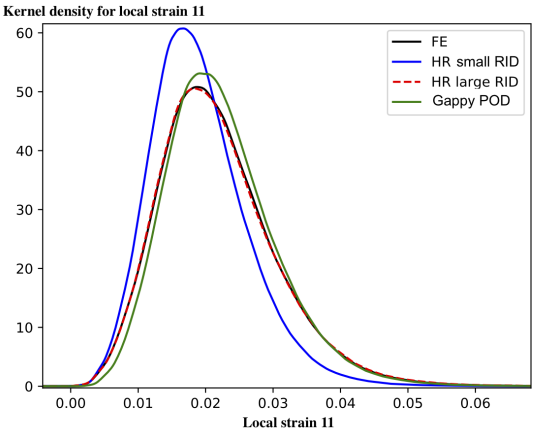

Fig. 6: Kernel of the probability density function for Gauss point values of ε_{11} and σ_{11} at the tensile peak of the 200th cycle.

The computational requirements to recover the strain field over 200 cycles can be viewed in table 3 where the numbers related to the original full field data have been also reported. The original FE simulation takes 1034 hours. It should be noted that the number of parallel processors utilized in this study have been arbitrarily chosen. For the full field simulation 24 processors were selected because that is the maximum number available on each cluster node. For the HROM and Hybrid simulations, four processors were used each. The computational time for the recovery of the full strain field via hyperreduction was 27 hours for the small RID while for the large RID it took 38 hours. Although the time to run the hyperreduction on the large RID was 40% longer, much better prediction in strain was achieved. The storage requirement for the pruned data is almost the same for both RIDs. It is less than 7% of the original storage space. This storage space is occupied by the reduced bases $\boldsymbol{V}$ and $\boldsymbol{V}^{\epsilon}$. Therefore, by deleting the data outside the larger RID we save 93% of storage space, the recovery of the full strain field takes 38 hours and its accuracy is higher than 99%. The recovery based on FE strain over the RID and the Gappy POD is the fastest recovery procedure. But it does not enable data extrapolation.

-	Original FE data	Gappy POD	Small RID	Large RID
Nodes	1174719	19942	19942	35893
Elements	859848	9286	9286	17381
Computation time x processors	1034 h x 24	0.08 h x 1	27 h x 4	38 h x 4
Storage memory Gbs	101.	5.	3.5	3.5
E_{11} (error)	0.019	0.02 (5%)	0.017 (10%)	0.019 ($< 1\%$)
Std deviation for ε_{11} (error)	0.84	0.88 (5%)	0.86 (2%)	0.84 ($< 1\%$)

Table 3: Finite element mesh details and the resources needed to run the full field, hyperreduced and Gappy POD, predictions.

5 Conclusion

Crystalline plasticity modeling is fed by experimental data and large volumes of simulated data. Erasing simulation data to free up memory space becomes necessary as more and more mechanical tests are performed. But there is a risk in erasing data: the risk of not being able to investigate modeling issues further once the data has been erased. In the present paper, we show that the data pruning we have developed allows to reduce the volume of data saved in storage system while keeping the possibility to evaluate the strain-ratcheting phenomenon. It is a very complex phenomenon, depending on the loading conditions applied to a polycrystal and the mechanical behavior of each grain. The recovery procedure of strain fields involves physical governing equations. It is nevertheless 27 times faster than the original FE simulation and it uses 8 times less computational resources. Simulation data in crystal plasticity have been compressed to 3% of their original size with approximation error lower than 1%. Results show the capability of choosing the size of the pruned data via the extent of the reduced integration domain involve in the hyperreduction method. This pruning method has extrapolation capabilities. In this paper, the input data of the pruning algorithm are related to 10 cycles of a cyclic simulation. After the data pruning, the recovery procedure has accurately extrapolated the pruned data up to 200 cycles.

The hyper-reduction scheme involved in the data pruning procedure has shown its accuracy when considering various parameter variations such as loading parameter or constitutive coefficients. The method can be applied to even more complex loading conditions, including multiaxial mechanical testing, and to other microstructures of composite materials. In the related works in progress we investigate the insertion of defect in the reduced integration domain in order to evaluate stress variations due to defects.

6 Appendix

Algorithm 1: k-SWIM Selection of Variables with EmpIrical Modes

Input : integer k, linearly independent empirical modes $\boldsymbol{v}_l \in \mathbb{R}^d$, $l = 1, \ldots, M$

Output: variables index set $\mathcal{P}^{(k)}$

set $\mathcal{P}_0 := \emptyset$, $j = 0$, $\boldsymbol{U}_1 = [\,]$; `// initialization`

for $l = 1, \ldots, M$ **do**

  $\boldsymbol{r}_l \leftarrow \boldsymbol{v}_l - \boldsymbol{U}_l \left((\boldsymbol{U}_l[\mathcal{P}_j, :])^T \boldsymbol{U}_l[\mathcal{P}_j, :] \right)^{-1} (\boldsymbol{U}_l[\mathcal{P}_j, :])^T \boldsymbol{v}_l[\mathcal{P}_j]$; `// residual vector`

  for $n = 1, \ldots, k$ **do**

    $j \leftarrow j + 1$; `// add the k largest value of the residual`

    $i_j \leftarrow \arg\max_{i \in \{1,\ldots,d\} \setminus \mathcal{P}_{j-1}} |\boldsymbol{r}_I[i]|$; `// index selection`

    $\boldsymbol{r}_l[i_j] \leftarrow 0$; `// variable already selected`

    $\mathcal{P}_j \leftarrow \mathcal{P}_{j-1} \cup \{i_j\}$; `// extend index set`

  $\boldsymbol{U}_{l+1} \leftarrow [\boldsymbol{v}_1, \ldots, \boldsymbol{v}_l]$; `// truncated reduced matrix`

set $\mathcal{P}^{(k)} := \mathcal{P}_j$.

7 Acknowledgements

This work was supported by Safran via the sponsorship chair Cristal.

References

1. Alharbi, H.F., Kalidindi, S.R.: Crystal plasticity finite element simulations using a database of discrete fourier transforms. International Journal of Plasticity **66**, 71 – 84 (2015). DOI https://doi.org/10.1016/j.ijplas.2014.04.006. URL `http://www.sciencedirect.com/science/article/pii/S0749641914000898`. Plasticity of Textured Polycrystals In Honor of Prof. Paul Van Houtte
2. Bacry, E., Gaffas, S., Leroy, F., Morel, M., Nguyen, D.P., Sebiat, Y., Sun, D.: Scalpel3: A scalable open-source library for healthcare claims databases. International Journal of Medical Informatics **141**, 104203 (2020). DOI https://doi.org/10.1016/j.ijmedinf.2020.104203. URL `http://www.sciencedirect.com/science/article/pii/S1386505619312493`
3. Barrault, M., Maday, Y., Nguyen, N., Patera, A.: An 'empirical interpolation' method: application to efficient reduced-basis discretization of partial differential equations. C. R. Math. Acad. Sci. Paris Series I **339**, 667–672 (2004)
4. Bashtannyk, D., Hyndman, R.: Bandwidth selection for kernel conditional density estimation. Computational Statistics & Data Analysis **36**, 279–298 (2001)
5. Besson, J., Cailletaud, G., Chaboche, J., Forest, S.: Non-linear mechanics of materials, vol. 167. Springer (2009)
6. Busso, E.P., Cailletaud, G.: On the selection of active slip systems in crystal plasticity. International Journal of Plasticity **21**(11), 2212 – 2231 (2005). Plasticity of Heterogeneous Materials
7. Chaturantabut, S., Sorensen, D.: Nonlinear model reduction via discrete empirical interpolation. SIAM Journal on Scientific Computing **32**(5), 2737–2764 (2010)

8. Cruzado, A., LLorca, J., Segurado, J.: Modeling cyclic deformation of inconel 718 superalloy by means of crystal plasticity and computational homogenization. International Journal of Solids and Structures **122-123**, 148 – 161 (2017). DOI 10.1016/j.ijsolstr.2017.06.014
9. Everson, R., Sirovich, L.: Karhunen-Loève procedure for gappy data. J. Opt. Soc. Am. A **12**, 1657–1664 (1995)
10. Farhat, C., Avery, P., Chapman, T., Cortial, J.: Dimensional reduction of nonlinear finite element dynamic models with finite rotations and energy-based mesh sampling and weighting for computational efficiency. International Journal for Numerical Methods in Engineering **98(9)**, 625–662 (2014)
11. Farooq, H., Cailletaud, G., Forest, S., Ryckelynck, D.: Crystal plasticity modeling of the cyclic behavior of polycrystalline aggregates under non-symmetric uniaxial loading: Global and local analyses. International Journal of Plasticity **126**, 102619 (2019). DOI 10.1016/j.ijplas.2019.10.007
12. Fauque, J., Ramière, I., Ryckelynck, D.: Hybrid hyper?reduced modeling for contact mechanics problems. International journal for numerical methods in engineering **115**(1), 309–317 (2018). DOI 10.1002/nme.5798. URL `https://doi.org/10.1002/nme.5798`
13. Forest, S., Rubin, M.: A rate-independent crystal plasticity model with a smooth elastic-plastic transition and no slip indeterminacy. European Journal of Mechanics - A/Solids **55**, 278 – 288 (2016)
14. Frankel, A., Jones, R., Alleman, C., Templeton, J.: Predicting the mechanical response of oligocrystals with deep learning. Computational Materials Science **169**, 109099 (2019). DOI https://doi.org/10.1016/j.commatsci.2019.109099. URL `http://www.sciencedirect.com/science/article/pii/S0927025619303908`
15. Fritzen, F., Hassani, M.: Space–time model order reduction for nonlinear viscoelastic systems subjected to long-term loading. Meccanica **53**(6), 1333–1355 (2018)
16. Gérard, C., Cailletaud, G., Bacroix, B.: Modeling of latent hardening produced by complex loading paths in FCC alloys. International Journal of Plasticity **42**, 194 – 212 (2013)
17. Gu, T., Medy, J.R., Klosek, V., Castelnau, O., Forest, S., Herv-Luanco, E., LecouturierDupouy, F., Proudhon, H., Renault, P.O., Thilly, L., Villechaise, P.: Multiscale modeling of the elasto-plastic behavior of architectured and nanostructured Cu-Nb composite wires and comparison with neutron diffraction experiments. International Journal of Plasticity (2019)
18. Hernández, J., Oliver, J., Huespe, A., Caicedo, M., Cante, J.: High-performance model reduction techniques in computational multiscale homogenization. Computer Methods in Applied Mechanics and Engineering **276**, 149 – 189 (2014)
19. Hilth, W., Ryckelynck, D., Menet, C.: Data pruning of tomographic data for the calibration of strain localization models. Mathematical and Computational Applications **24**(1) (2019)
20. Kanit, T., Forest, S., Galliet, I., Mounoury, V., Jeulin, D.: Determination of the size of the representative volume element for random composites: statistical and numerical approach. International Journal of Solids and Structures **40**(13), 3647 – 3679 (2003)
21. Karhunen, K.: Zur spektraltheorie stochastischer prozesse. Ann. Acad. Sci. Finnicae, Ser. A **1**, 34 (1946)
22. Kotha, S., Ozturk, D., Ghosh, S.: Parametrically homogenized constitutive models (phcms) from micromechanical crystal plasticity fe simulations, part i: Sensitivity analysis and parameter identification for titanium alloys. International Journal of Plasticity **120**, 296 – 319 (2019)
23. Liu, Z., Bessa, M., Liu, W.K.: Self-consistent clustering analysis: An efficient multi-scale scheme for inelastic heterogeneous materials. Computer Methods in Applied Mechanics and Engineering **306**, 319 – 341 (2016). DOI https://doi.org/10.1016/j.cma.2016.04.004. URL `http://www.sciencedirect.com/science/article/pii/S0045782516301499`
24. Loève, M.: Probability Theory. The university series in higher mathematics, NJ, 3rd edition. Van Nosterand, Princeton (1963)
25. Masui, K., Amiri, M., Connor, L., Deng, M., Fandino, M., Höfer, C., Halpern, M., Hanna, D., Hincks, A., Hinshaw, G., Parra, J., Newburgh, L., Shaw, J., Vanderlinde, K.: A compression scheme for radio data in high performance computing. Astronomy

and Computing **12**, 181 – 190 (2015). DOI https://doi.org/10.1016/j.ascom.2015.07.002. URL http://www.sciencedirect.com/science/article/pii/S2213133715000694
26. Matou, K., Geers, M.G., Kouznetsova, V.G., Gillman, A.: A review of predictive nonlinear theories for multiscale modeling of heterogeneous materials. Journal of Computational Physics **330**, 192 – 220 (2017)
27. Méric, L., Poubanne, P., Cailletaud, G.: Single crystal modeling for structural calculations: part 1 – model presentation. J. Eng. Mater. Technol. **113** (1991)
28. Michel, J., Suquet, P.: Nonuniform transformation field analysis. International Journal of Solids and Structures **40**(25), 6937 – 6955 (2003)
29. N. Lorenz, E.: Empirical orthogonal functions and statistical weather prediction. Statistical Forecasting **1** (1956)
30. Pelle, J.P., Ryckelynck, D.: An efficient adaptive strategy to master the global quality of viscoplastic analysis. Computers & Structures **78**(1), 169 – 183 (2000)
31. Prithivirajan, V., Sangid, M.D.: The role of defects and critical pore size analysis in the fatigue response of additively manufactured in718 via crystal plasticity. Materials & Design **150**, 139 – 153 (2018)
32. Rovinelli, A., Sangid, M.D., Proudhon, H., Guilhem, Y., Lebensohn, R.A., Ludwig, W.: Predicting the 3d fatigue crack growth rate of small cracks using multimodal data via bayesian networks: In-situ experiments and crystal plasticity simulations. Journal of the Mechanics and Physics of Solids **115**, 208 – 229 (2018). DOI https://doi.org/10.1016/j.jmps.2018.03.007. URL http://www.sciencedirect.com/science/article/pii/S0022509617310839
33. Ryckelynck, D.: A priori hyperreduction method: an adaptive approach. Journal of Computational Physics **202**(1), 346 – 366 (2005)
34. Ryckelynck, D.: Hyper-reduction of mechanical models involving internal variables. International Journal for Numerical Methods in Engineering **77**(1), 75–89 (2009)
35. Ryckelynck, D., Lampoh, K., Quilici, S.: Hyper-reduced predictions for lifetime assessment of elasto-plastic structures. Meccanica **51**(2), 309–317 (2016). DOI 10.1007/s11012-015-0244-7. URL https://doi.org/10.1007/s11012-015-0244-7
36. Ryckelynck, D., Missoum-Benziane, D., Musienko, A., Cailletaud, G.: Toward "green" mechanical simulations in materials science : hyper-reduction of a polycrystal plasticity model. Revue Européenne de Mécanique Numérique/European Journal of Computational Mechanics **19**(4), 365–388 (2010)
37. Rycroft, C.: Voro++: a three-dimensional voronoi cell library in C++. Chaos **19** (2009). DOI 10.1063/1.3215722
38. Sedighiani, K., Diehl, M., Traka, K., Roters, F., Sietsma, J., Raabe, D.: An efficient and robust approach to determine material parameters of crystal plasticity constitutive laws from macro-scale stressstrain curves. International Journal of Plasticity **134**, 102779 (2020). DOI https://doi.org/10.1016/j.ijplas.2020.102779. URL http://www.sciencedirect.com/science/article/pii/S0749641919308769
39. Shantsev, D.V., Jaysaval, P., de la Kethulle de Ryhove, S., Amestoy, P.R., Buttari, A., LExcellent, J.Y., Mary, T.: Large-scale 3-D EM modelling with a Block Low-Rank multifrontal direct solver. Geophysical Journal International **209**(3), 1558–1571 (2017)
40. Sirovich, L.: Turbulence and the dynamics of coherent structures, Parts I, II and III. Quarterly of Applied Mathematics **XLV**(3), 561 – 590 (1987)
41. Sun, F., Meade, E.D., ODowd, N.P.: Microscale modelling of the deformation of a martensitic steel using the voronoi tessellation method. Journal of the Mechanics and Physics of Solids **113**, 35 – 55 (2018)
42. Virtanen, P., Gommers, R., Oliphant, T.E., Haberland, M., Reddy, T., Cournapeau, D., Burovski, E., Peterson, P., Weckesser, W., Bright, J., van der Walt, S.J., Brett, M., Wilson, J., Jarrod Millman, K., Mayorov, N., Nelson, A.R.J., Jones, E., Kern, R., Larson, E., Carey, C., Polat, İ., Feng, Y., Moore, E.W., Vand erPlas, J., Laxalde, D., Perktold, J., Cimrman, R., Henriksen, I., Quintero, E.A., Harris, C.R., Archibald, A.M., Ribeiro, A.H., Pedregosa, F., van Mulbregt, P., Contributors, S...: SciPy 1.0: Fundamental Algorithms for Scientific Computing in Python. Nature Methods **17**, 261–272 (2020). DOI https://doi.org/10.1038/s41592-019-0686-2
43. Yagawa, G., Shioya, R.: Parallel finite elements on a massively parallel computer with domain decomposition. Computing Systems in Engineering **4**(4), 495 – 503 (1993). Parallel Computational Methods for Large-Scale Structural Analysis and Design

503 44. Z–set package: Non-linear material & structure analysis suite, www.zset-software.com
504 (2013)
505 45. Zhang, H., Diehl, M., Roters, F., Raabe, D.: A virtual laboratory using high resolu-
506 tion crystal plasticity simulations to determine the initial yield surface for sheet metal
507 forming operations. International Journal of Plasticity **80**, 111 – 138 (2016)